

AN OPEN-ENDED CIRCULAR WAVEGUIDE WITH AN INFINITE CONDUCTING FLANGE COVERED BY A DIELECTRIC HEMI-SPHERICAL RADOME SHELL: FULL-WAVE ANALYSIS AND GREEN DYADICS

L. W. Li, L. Zhou, M. S. Leong, T. S. Yeo, and P. S. Kooi

Communications and Microwave Division
Department of Electrical Engineering
National University of Singapore
10 Kent Ridge Crescent, Singapore 119260

- 1. Introduction**
 - 2. Basic Formulation of the Problem**
 - 3. Expressions of Dyadic Green's Functions in Five Regions**
 - 4. Determination of Scattering Coefficients of DGFs Using Boundary Conditions**
 - A Boundary Conditions on Hemi-Spherical Interfaces
 - B Boundary Conditions on the Aperture $z = 0$ or $\theta = \pi/2$
 - 5. Fraunhofer Field Expressions in Far-Zone**
 - 6. Numerical Discussions on Effects of Aperture-Radome Interaction**
 - 7. Concluding Remarks**
 - A Orthogonal Relations of the Conical Vector Wave Functions
 - B Orthogonal Relations of Cylindrical Vector Wave Functions
- Acknowledgment
References

1. INTRODUCTION

It is well-known that apertures have been considered as the most important microwave antenna, as introduced in the conventional antenna text books [1–3], and that such microwave antennas are usually fed by waveguides of either rectangular and circular cross sections. Because of its simple structure and ease of manufacture as well as because of the field symmetry during the antenna scanning, the aperture antenna fed by a circular waveguide with an infinite conducting flange is of practical use. In the aforementioned text books, the current distribution over the aperture is assumed as either a constant [1, 2, 4] or a waveguide-generated dominant-mode [1, 5].

With a generalized representation of dyadic Green's functions (DGFs) for multi-layered media given by Li et al. [6], the electromagnetic fields in a three-layered geometry due to an aperture antenna of a known constant current distribution covered by a hemi-spherical radome shell has been considered [4]. Then, a more practical field distribution over the aperture, i.e., the dominant TE_{11} mode excitation generated by a circular waveguide, has been further taken into account as an improvement of the current distribution over the aperture [7]. This work was further extended to the analysis of the isotropic radome fed by an off-centered aperture source [8]. Recently, a further improvement has been achieved [9] by modifying the aperture's magnetic current distribution due to the near-field interaction and by employing the reactive interaction procedure. However, the above analysis does not include all the re-excited modes inside the waveguide due to the aperture mainly due to the difficulty of the geometry involving both cylindrical and spherical structures. Although the circular waveguide feeding has been considered in the authors' previous studies on the antenna radome performance, the image theory and the given current distribution over the aperture opening have been assumed. So far, an exact analysis of such a geometry, where all the modes are considered in the matching of boundary conditions on all the conducting walls and dielectric interfaces, is still unavailable.

This paper presents a fullwave rigorous analysis of electromagnetic radiation of a dipole antenna located in a circular open waveguide. The waveguide flange is then flushed mounted on an infinite ground plane and then covered by a dielectric spherical-shell radome (see Figure 1). To conveniently solve the problem, the physical structure is separated into five regions. For these regions, dyadic Green's functions are for-

mulated in terms of the spherical vector wave functions in the first four regions and the cylindrical vector wave functions in the fifth region. The third and fourth regions are separated because of the future ease of determination of the power patterns which need not the coordinates transform. In the analysis, all the possible modes are included and all the conducting walls and (imaginary) dielectric interfaces are considered. Although coupled to each other, the scattering coefficients of these DGFs are formulated in compact matrix form by using the mode-matching technique and applying the method of scattering superposition. The antenna patterns of the radiating system in the far zone are obtained and various effects due to different radome thicknesses, dimensions, and radius of the feed waveguide are discussed in detail.

2. BASIC FORMULATION OF THE PROBLEM

The geometry of the problem is illustrated in Fig. 1 where the waveguide opening aperture is excited by a dipole antenna located inside the circular waveguide, mounted on the ground plane, and covered by a dielectric hemi-spherical radome shell. For convenience of the analysis, an imaginary hemi-spherical interface at $r = r_0$ and a interface of the circular waveguide opening are assumed. Therefore, the structure is divided into the five regions, as shown in Fig. 1.

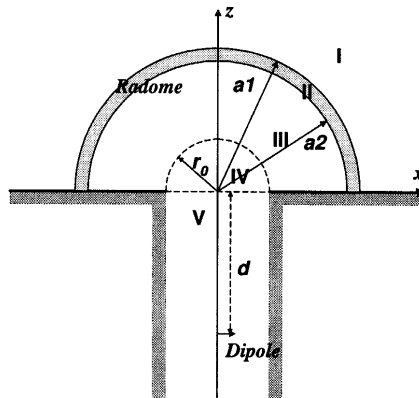


Figure 1. A circular waveguide-fed aperture mounted on an infinite ground plane and covered by a dielectric hemi-spherical shell.

The radiated electromagnetic fields, \mathbf{E}_f and \mathbf{H}_f in the f -th region ($f = I, \dots, V$), contributed by an electric current distribution \mathbf{J}_s lying in the fifth region may be expressed by

$$\nabla \times \nabla \times \mathbf{E}_f(\mathbf{r}) - k_0^2 \mathbf{E}_f(\mathbf{r}) = i\omega\mu_0 \mathbf{J}_f(\mathbf{r}')\delta_{f5}, \quad (1a)$$

$$\nabla \times \nabla \times \mathbf{H}_f(\mathbf{r}) - k_0^2 \mathbf{H}_f(\mathbf{r}) = (\nabla \times \mathbf{J})_f(\mathbf{r}')\delta_{f5}, \quad (1b)$$

where δ_{fs} ($= 1$ for $s = f$ and 0 for $s \neq f$) denotes the Kronecker delta, while $k_0 = \omega\sqrt{\mu_0\varepsilon_0}$, ε_f , and μ_0 identify the propagation constant, the permittivity, and the permeability in free-space, respectively. A time dependence $\exp(-i\omega t)$ is assumed for the field expressions throughout the paper.

Since the above equations are linear, the electric and magnetic fields \mathbf{E}_f and \mathbf{H}_f due to such an electric current source can be obtained as follows:

$$\mathbf{E}_f(\mathbf{r}) = i\omega\mu_f \iiint_{V_s} \overline{\mathbf{G}}_e^{(f5)}(\mathbf{r}, \mathbf{r}') \cdot \mathbf{J}_s(\mathbf{r}') dV', \quad (2a)$$

$$\mathbf{H}_f(\mathbf{r}) = \iiint_{V_s} \nabla \times \overline{\mathbf{G}}_e^{(f5)}(\mathbf{r}, \mathbf{r}') \cdot \mathbf{J}_s(\mathbf{r}') dV', \quad (2b)$$

where V_s identifies the volume occupied by the sources in the fifth region. Substituting Eq. (2) into (1a) yields

$$\nabla \times \nabla \times \overline{\mathbf{G}}_e^{(f5)}(\mathbf{r}, \mathbf{r}') - k_0^2 \overline{\mathbf{G}}_e^{(f5)}(\mathbf{r}, \mathbf{r}') = \overline{\mathbf{I}}\delta(\mathbf{r} - \mathbf{r}')\delta_{f5}, \quad (3)$$

where $\overline{\mathbf{I}}$ is the identity dyadic and $\delta(\mathbf{r} - \mathbf{r}')$ the Dirac delta function.

On dielectric interfaces, the electric type of dyadic Green's function $\overline{\mathbf{G}}_e^{(f5)}(\mathbf{r}, \mathbf{r}')$ hence satisfies the following boundary conditions at the hemi-spherical interface:

$$\hat{\mathbf{r}} \times \overline{\mathbf{G}}_e^{(f5)} \Big|_{r=r_f} = \hat{\mathbf{r}} \times \overline{\mathbf{G}}_e^{[(f+1)5]} \Big|_{r=r_f}, \quad (4a)$$

$$\frac{1}{\mu_f} \hat{\mathbf{r}} \times \nabla \times \overline{\mathbf{G}}_e^{(f5)} \Big|_{r=r_f} = \frac{1}{\mu_{f+1}} \hat{\mathbf{r}} \times \nabla \times \overline{\mathbf{G}}_e^{[(f+1)5]} \Big|_{r=r_f}. \quad (4b)$$

with $f = 1, 2,$ and 3 and

$$r_1 = a_1, \quad r_2 = a_2, \quad r_3 = r_0. \quad (5)$$

and the following boundary conditions at the aperture interface between regions IV and V ($z = 0$ in cylindrical coordinates or $\theta = 90^\circ$ in spherical coordinates):

$$\hat{\boldsymbol{\theta}} \times \overline{\mathbf{G}}_e^{(45)} \Big|_{\theta=90^\circ} = -\hat{\mathbf{z}} \times \overline{\mathbf{G}}_e^{(55)} \Big|_{z=0}, \tag{6a}$$

$$\frac{1}{\mu_4} \hat{\boldsymbol{\theta}} \times \nabla \times \overline{\mathbf{G}}_e^{(45)} \Big|_{\theta=90^\circ} = -\frac{1}{\mu_5} \hat{\mathbf{z}} \times \nabla \times \overline{\mathbf{G}}_e^{(55)} \Big|_{z=0}. \tag{6b}$$

For TE- and TM-modes, the electric type of dyadic Green's function, $\overline{\mathbf{G}}_e^{(fs)}(\mathbf{r}, \mathbf{r}')$, satisfies the Dirichlet and Neumann boundary conditions respectively on the conducting ground $\theta = 90^\circ$ (regions I, II, and III) and on the conducting wall of the circular waveguide $\rho = r_0$ (region V):

$$\hat{\boldsymbol{\theta}} \times \overline{\mathbf{G}}_e^{(f5)} \Big|_{\theta=90^\circ} = 0, \quad \text{for } f = 1, 2, 3; \tag{7a}$$

$$\hat{\boldsymbol{\rho}} \times \overline{\mathbf{G}}_e^{(55)} \Big|_{\rho=r_0} = 0. \tag{7b}$$

Since the electric and magnetic types of dyadic Green's functions are dual, the electric type of dyadic Green's function $\overline{\mathbf{G}}_e^{(f5)}(\mathbf{r}, \mathbf{r}')$ can be converted to the magnetic type $\overline{\mathbf{G}}_m^{(f5)}(\mathbf{r}, \mathbf{r}')$ or vice versa by making the simple replacement $\mathbf{E} \rightarrow \mathbf{H}$, $\mathbf{H} \rightarrow -\mathbf{E}$, $\mathbf{J} \rightarrow \mathbf{M}$, $\mathbf{M} \rightarrow -\mathbf{J}$, $\mu \rightarrow \varepsilon$, and $\varepsilon \rightarrow \mu$. To avoid unnecessary repetition, only the electric type of dyadic Green's function will be presented in this paper.

3. EXPRESSIONS OF DYADIC GREEN'S FUNCTIONS IN FIVE REGIONS

To formulate the electromagnetic dyadic Green's functions in the five regions shown in Fig. 1, both the spherical and cylindrical vector wave functions as introduced by [10–12] will be utilized in this paper.

For expressing the electromagnetic fields and dyadic Green's functions, we define the following vector eigenfunctions using the same notations as those shown by Tai [12] for spherical coordinates (in regions I, II, III and IV):

$$\begin{aligned} \mathbf{M}_{e_{mn}}(k) = & \mp \frac{m}{\sin \theta} z_n(kr) P_n^m(\cos \theta) \frac{\sin(m\phi)}{\cos} \hat{\boldsymbol{\theta}} \\ & - z_n(kr) \frac{dP_n^m(\cos \theta)}{d\theta} \frac{\cos(m\phi)}{\sin} \hat{\boldsymbol{\phi}}, \end{aligned} \tag{8a}$$

$$\begin{aligned}
 \mathbf{N}_{\varepsilon mn}(k) &= \frac{n(n+1)}{kr} z_n(kr) P_n^m(\cos\theta) \frac{\cos(m\phi)}{\sin} \hat{\mathbf{r}} \\
 &+ \frac{1}{kr} \frac{d[rz_n(kr)]}{dr} \left[\frac{dP_n^m(\cos\theta)}{d\theta} \frac{\cos(m\phi)}{\sin} \hat{\boldsymbol{\theta}} \right. \\
 &\left. \mp \frac{m}{\sin\theta} P_n^m(\cos\theta) \frac{\sin(m\phi)}{\cos} \hat{\boldsymbol{\phi}} \right], \tag{8b}
 \end{aligned}$$

where $z_n(kr)$ denotes the spherical Bessel function of n -order, $P_n^m(\cos\theta)$ identifies the associated Legendre function of the first kind with the order (n, m) , and for cylindrical coordinates (in region V):

$$\begin{aligned}
 \mathbf{M}_{\varepsilon m\nu}(h) &= \left[\mp \frac{mJ_m(\nu\rho)}{\rho} \frac{\sin(m\phi)}{\cos} \hat{\boldsymbol{\rho}} \right. \\
 &\left. - \frac{dJ_m(\nu\rho)}{d\rho} \frac{\cos(m\phi)}{\sin} \hat{\boldsymbol{\phi}} \right] e^{ihz}, \tag{9a}
 \end{aligned}$$

$$\begin{aligned}
 \mathbf{N}_{\varepsilon m\lambda}(h) &= \frac{1}{k\lambda} \left[ih \frac{dJ_m(\lambda\rho)}{d\rho} \frac{\cos(m\phi)}{\sin} \hat{\boldsymbol{\rho}} \right. \\
 &\mp \frac{ihm}{r} J_m(\lambda\rho) \frac{\sin(m\phi)}{\cos} \hat{\boldsymbol{\phi}} \\
 &\left. + \lambda^2 J_m(\lambda\rho) \frac{\cos(m\phi)}{\sin} \hat{\boldsymbol{z}} \right] e^{ihz} i, \tag{9b}
 \end{aligned}$$

where

$$\nu = \frac{q_{mn}}{r_0}, \tag{10a}$$

$$\lambda = \frac{p_{mn}}{r_0}, \tag{10b}$$

with q_{mn} and p_{mn} as roots of

$$\begin{aligned}
 \left. \frac{dJ_m(x)}{dx} \right|_{x=\nu} &= 0 \text{ (for TE}_{mn}\text{- modes), } k_\nu = \sqrt{h^2 + \nu^2}; \\
 J_m(x)|_{x=\lambda} &= 0 \text{ (for TM}_{mn}\text{- modes), } k_\lambda = \sqrt{h^2 + \lambda^2}.
 \end{aligned}$$

The parameter r_0 is the radius of the conducting circular waveguide.

The above vector wave functions have been verified by Tai [12] to be orthogonal among themselves as well as with respect to each other as they are integrated over all the values of ρ , ϕ , and z in cylindrical coordinates and r , θ , and ϕ in spherical coordinates.

Applying the method of contour integration in the complex h -plane, and following the similar way of constructing the dyadic Green's function for spherical structures by [12], we define, for the current source located in the region V , the dyadic Green's function in regions I, II, III, and IV with the spherical Bessel and Hankel functions as follows:

$$\begin{aligned} \overline{\mathbf{G}}_{es}^{(f5)}(\mathbf{r}, \mathbf{r}') = & \frac{ik_s}{4\pi} \sum_{n=0}^{\infty} \sum_{m=0}^n (2 - \delta_m^0) \frac{2n+1}{n(n+1)} \frac{(n-m)!}{(n+m)!} \\ & \cdot \left[(1 - \delta_f^4) \mathbf{M}_{\epsilon mn}^{(1)}(k_f) \mathcal{A}_M^{f5} \mathbf{M}'_{\epsilon m\nu}(-k_\nu) \right. \\ & + (1 - \delta_f^4) \mathbf{N}_{\epsilon mn}^{(1)}(k_f) \mathcal{A}_N^{f5} \mathbf{N}'_{\epsilon m\lambda}(-k_\lambda) \\ & + (1 - \delta_f^1) \mathbf{M}_{\epsilon mn}(k_f) \mathcal{B}_M^{f5} \mathbf{M}'_{\epsilon m\nu}(-k_\nu) \\ & \left. + (1 - \delta_f^1) \mathbf{N}_{\epsilon mn}(k_f) \mathcal{B}_N^{f5} \mathbf{N}'_{\epsilon m\lambda}(-k_\lambda) \right], \end{aligned} \quad (11)$$

where the prime denotes the coordinates (r', θ', ϕ') of the current source $\mathbf{J}_s(\mathbf{r}')$, m and n identify the eigenvalue parameters in spherical coordinates while ν and λ represent the eigenvalues in circular cylindrical coordinates, $\mathbf{M}_{\epsilon mn}$ stands for the electric field of the TE $_{mn}$ mode while $\mathbf{N}_{\epsilon mn}$ represents that of the TM $_{mn}$ mode, and $\mathcal{A}_{M,N}^{f5}$ and $\mathcal{B}_{M,N}^{f5}$ are the scattering coefficients of dyadic Green's function to be solved for.

Both the spherical and cylindrical vector wave functions are used in the representation to express the electromagnetic fields due to the given source current distribution. The superscript (1) denotes that the third-type spherical or cylindrical Bessel function or the first-type spherical or cylindrical Hankel function $h_n^{(1)}(\rho)$ should be chosen in the expression of the spherical wave vector functions. For the rest of the vector wave functions, we should still choose the normal first-type spherical Bessel function $J_n(\rho)$.

As for regions I, II and III, in order to satisfy the boundary conditions on the ground plane, we have to assume

$$n = \begin{cases} q, & q + m = \text{even for } \mathbf{M}_{\epsilon mn}\text{-mode;} \\ p, & p + m = \text{odd for } \mathbf{N}_{\epsilon mn}\text{-mode.} \end{cases} \quad (12)$$

Using the method of scattering superposition, we consider the dyadic Green's function in region V as the sum of an infinite waveguide DGF

and a scattering DGF. The dyadic Green's function is therefore given by [13]:

$$\overline{\mathbf{G}}_e^{(55)}(\mathbf{r}, \mathbf{r}') = \overline{\mathbf{G}}_{0e}(\mathbf{r}, \mathbf{r}') + \overline{\mathbf{G}}_{es}^{(55)}(\mathbf{r}, \mathbf{r}') \quad (13)$$

where the infinite waveguide DGF can be expressed [12] for $z \gtrless z'$ as

$$\begin{aligned} \overline{\mathbf{G}}_{0e}(\mathbf{r}, \mathbf{r}') &= -\frac{\hat{z}\hat{z}}{k_0^2} \delta(\mathbf{r} - \mathbf{r}') \\ &+ \sum_{m,n} \left[\frac{i(2 - \delta_{m0})}{4\pi\nu^2 I_\nu k_\nu} \mathbf{M}_{\circ m\nu}(\pm k_\nu) \mathbf{M}'_{\circ m\nu}(\mp k_\nu) \right. \\ &\left. + \frac{i(2 - \delta_{m0})}{4\pi\lambda^2 I_\lambda k_\lambda} \mathbf{N}_{\circ m\lambda}(\pm k_\lambda) \mathbf{N}'_{\circ m\lambda}(\mp k_\lambda) \right], \end{aligned} \quad (14)$$

and the scattering DGF can be therefore expressed for $z \gtrless z'$ as

$$\begin{aligned} \overline{\mathbf{G}}_{es}^{(55)}(\mathbf{r}, \mathbf{r}') &= \sum_{m,n} \left[\frac{i(2 - \delta_{m0})}{4\pi\nu^2 I_\nu k_\nu} C_{m\nu}^M \mathbf{M}_{\circ m\nu}(\pm k_\nu) \mathbf{M}'_{\circ m\nu}(\mp k_\nu) \right. \\ &\left. + \frac{i(2 - \delta_{m0})}{4\pi\lambda^2 I_\lambda k_\lambda} C_{m\nu}^N \mathbf{N}_{\circ m\lambda}(\pm k_\lambda) \mathbf{N}'_{\circ m\lambda}(\mp k_\lambda) \right], \end{aligned} \quad (15)$$

in which the eigenvalues ν and λ have been given previously in (9) and the two parameters I_ν and I_λ are given respectively by

$$I_\nu = \int_0^{r_0} J_n^2(\nu\rho) \rho d\rho = \frac{r_0^2}{2\nu^2} \left[\frac{\partial J_n(\nu\rho)}{\partial \rho} \right]_{\rho=r_0}^2, \quad (16a)$$

$$I_\lambda = \int_0^{r_0} J_n^2(\lambda\rho) \rho d\rho = \frac{r_0^2}{2\lambda^2} \left[\frac{\partial J_n(\lambda\rho)}{\partial \rho} \right]_{\rho=r_0}^2. \quad (16b)$$

In different regions, it is assumed that the source contribution to the field at a given point remains, i.e.,

$$\begin{aligned} \begin{bmatrix} I_M^{\text{cost}} \\ I_N^{\text{cost}} \end{bmatrix} &= \iiint_{V_s} \begin{bmatrix} \mathbf{M}'(k_s) \\ \mathbf{N}'(k_s) \end{bmatrix} \cdot \mathbf{J}_s(\mathbf{r}') dV' \\ &= \text{constant matrix.} \end{aligned} \quad (17)$$

Therefore, $\mathbf{M}'(k_s)$ and $\mathbf{N}'(k_s)$ for $r \gtrless r'$ (in regions I, II, III and IV)

or $z \gtrsim z'$ (in region V) can be expressed as

$$\begin{bmatrix} \mathbf{M}'(k_s) \\ \mathbf{N}'(k_s) \end{bmatrix} = \begin{cases} \begin{bmatrix} \mathbf{M}'_{\varepsilon mn}(-k_{1,2,3,4}) \\ \mathbf{N}'_{\varepsilon mn}(-k_{1,2,3,4}) \end{bmatrix}, \\ \text{Source in regions I, II, III and IV;} \\ \\ \begin{bmatrix} \mathbf{M}'_{\varepsilon m\nu}(\mp k_\nu) \\ \mathbf{N}'_{\varepsilon m\lambda}(-k_\lambda) \end{bmatrix}, \\ \text{Source in region V.} \end{cases} \quad (18)$$

As we do not intend to cover all the possibilities in this paper, we will concentrate on the antenna radiation in the conducting circular waveguide only.

4. DETERMINATION OF SCATTERING COEFFICIENTS OF DGFS USING BOUNDARY CONDITIONS

So far, we have constructed the dyadic Green's functions for every region with unknown scattering coefficients. To formulate these coefficients, boundary conditions are applied. It is immediately realized that these coefficients are coupled to each other. To solve for them for the structure is not as simple as that for the multilayered spherical structure where these coefficients can be decoupled.

A Boundary Conditions on Hemi-Spherical Interfaces

The boundary conditions satisfied by the dyadic Green's function have been shown in Eqs. (4a–7b). By applying the boundary condition (4a) and (4b) on the interfaces at $r = a_1$ and $r = a_2$ and by using the same method and procedure in [6], we obtain the following coefficient matrix equations:

$$\begin{aligned} & \begin{bmatrix} \hbar_{ff} \mathcal{A}_M^{fs} \\ \partial \hbar_{ff} \mathcal{A}_N^{fs} \end{bmatrix} + \begin{bmatrix} \mathfrak{S}_{ff} \mathcal{B}_M^{fs} \\ \partial \mathfrak{S}_{ff} \mathcal{B}_N^{fs} \end{bmatrix} \\ &= \begin{bmatrix} \hbar_{(f+1)f} \mathcal{A}_M^{(f+1)s} \\ \partial \hbar_{(f+1)f} \mathcal{A}_N^{(f+1)s} \end{bmatrix} + \begin{bmatrix} \mathfrak{S}_{(f+1)f} \mathcal{B}_M^{(f+1)s} \\ \partial \mathfrak{S}_{(f+1)f} \mathcal{B}_N^{(f+1)s} \end{bmatrix} \end{aligned} \quad (19)$$

and

$$\begin{aligned} & \frac{k_f}{\mu_f} \left[\frac{\partial \hbar_{ff} \mathcal{A}_M^{fs}}{\hbar_{ff} \mathcal{A}_N^{fs}} \right] + \frac{k_f}{\mu_f} \left[\frac{\partial \mathfrak{S}_{ff} \mathcal{B}_M^{fs}}{\mathfrak{S}_{ff} \mathcal{B}_N^{fs}} \right] \\ &= \frac{k_{f+1}}{\mu_{f+1}} \left[\frac{\partial \hbar_{(f+1)f} \mathcal{A}_M^{(f+1)s}}{\hbar_{(f+1)f} \mathcal{A}_N^{(f+1)s}} \right] + \frac{k_{f+1}}{\mu_{f+1}} \left[\frac{\partial \mathfrak{S}_{(f+1)f} \mathcal{B}_M^{(f+1)s}}{\mathfrak{S}_{(f+1)f} \mathcal{B}_N^{(f+1)s}} \right], \end{aligned} \quad (20)$$

where

$$\mathfrak{S}_{il} = j_n(k_i a_l), \quad (21a)$$

$$\hbar_{il} = h_n^{(1)}(k_i a_l), \quad (21b)$$

$$\partial \mathfrak{S}_{il} = \frac{1}{\rho} \frac{d[\rho j_n(\rho)]}{d\rho} \Big|_{\rho=k_i a_l}, \quad (21c)$$

$$\partial \hbar_{il} = \frac{1}{\rho} \frac{d[\rho h_n^{(1)}(\rho)]}{d\rho} \Big|_{\rho=k_i a_l}, \quad (21d)$$

with

$$l = 1, \text{ and } 2.$$

Using the method similar to that introduced by Li et al. for the planar, stratified media [14] and rewriting (19) and (20) into the simplified forms, we obtain

$$\left[\mathcal{A}_{M,N}^{(f+1)s} \right] = \frac{1}{\mathcal{T}_{Ff}^{H,V}} \left[\mathcal{A}_{M,N}^{fs} \right] + \frac{\mathcal{R}_{Ff}^{H,V}}{\mathcal{T}_{Ff}^{H,V}} \left[\mathcal{B}_{M,N}^{fs} \right], \quad (22a)$$

$$\left[\mathcal{B}_{M,N}^{(f+1)s} \right] = \frac{\mathcal{R}_{Pf}^{H,V}}{\mathcal{T}_{Pf}^{H,V}} \left[\mathcal{A}_{M,N}^{fs} \right] + \frac{1}{\mathcal{T}_{Pf}^{H,V}} \left[\mathcal{B}_{M,N}^{fs} \right], \quad (22b)$$

where

$$\mathcal{R}_{Pf}^H = \frac{\mu_f k_{f+1} \partial \hbar_{(f+1)f} \hbar_{ff} - \mu_{f+1} k_f \partial \hbar_{ff} \hbar_{(f+1)f}}{\mu_f k_{f+1} \mathfrak{S}_{ff} \partial \hbar_{(f+1)f} - \mu_{f+1} k_f \partial \mathfrak{S}_{ff} \hbar_{(f+1)f}}, \quad (23a)$$

$$\mathcal{R}_{Ff}^H = \frac{\mu_f k_{f+1} \partial \mathfrak{S}_{(f+1)f} \mathfrak{S}_{ff} - \mu_{f+1} k_f \partial \mathfrak{S}_{ff} \mathfrak{S}_{(f+1)f}}{\mu_f k_{f+1} \partial \mathfrak{S}_{(f+1)f} \hbar_{ff} - \mu_{f+1} k_f \mathfrak{S}_{(f+1)f} \partial \hbar_{ff}}, \quad (23b)$$

$$\mathcal{R}_{Pf}^V = \frac{\mu_f k_{f+1} \hbar_{(f+1)f} \partial \hbar_{ff} - \mu_{f+1} k_f \hbar_{ff} \partial \hbar_{(f+1)f}}{\mu_f k_{f+1} \partial \mathfrak{S}_{ff} \hbar_{(f+1)f} - \mu_{f+1} k_f \mathfrak{S}_{ff} \partial \hbar_{(f+1)f}}, \quad (23c)$$

$$\mathcal{R}_{Ff}^V = \frac{\mu_f k_{f+1} \mathfrak{S}_{(f+1)f} \partial \mathfrak{S}_{ff} - \mu_{f+1} k_f \mathfrak{S}_{ff} \partial \mathfrak{S}_{(f+1)f}}{\mu_f k_{f+1} \mathfrak{S}_{(f+1)f} \partial \bar{h}_{ff} - \mu_{f+1} k_f \partial \mathfrak{S}_{(f+1)f} \bar{h}_{ff}}, \quad (23d)$$

$$\mathcal{T}_{Pf}^H = \frac{\mu_f k_{f+1} (\mathfrak{S}_{(f+1)f} \partial \bar{h}_{(f+1)f} - \partial \mathfrak{S}_{(f+1)f} \bar{h}_{(f+1)f})}{\mu_f k_{f+1} \mathfrak{S}_{ff} \partial \bar{h}_{(f+1)f} - \mu_{f+1} k_f \partial \mathfrak{S}_{ff} \bar{h}_{(f+1)f}}, \quad (23e)$$

$$\mathcal{T}_{Ff}^H = \frac{\mu_f k_{f+1} (\partial \mathfrak{S}_{(f+1)f} \bar{h}_{(f+1)f} - \mathfrak{S}_{(f+1)f} \partial \bar{h}_{(f+1)f})}{\mu_f k_{f+1} \partial \mathfrak{S}_{(f+1)f} \bar{h}_{ff} - \mu_{f+1} k_f \mathfrak{S}_{(f+1)f} \partial \bar{h}_{ff}}, \quad (23f)$$

$$\mathcal{T}_{Pf}^V = \frac{\mu_f k_{f+1} (\partial \mathfrak{S}_{(f+1)f} \bar{h}_{(f+1)f} - \mathfrak{S}_{(f+1)f} \partial \bar{h}_{(f+1)f})}{\mu_f k_{f+1} \partial \mathfrak{S}_{ff} \bar{h}_{(f+1)f} - \mu_{f+1} k_f \mathfrak{S}_{ff} \partial \bar{h}_{(f+1)f}}, \quad (23g)$$

$$\mathcal{T}_{Ff}^V = \frac{\mu_f k_{f+1} (\mathfrak{S}_{(f+1)f} \partial \bar{h}_{(f+1)f} - \partial \mathfrak{S}_{(f+1)f} \bar{h}_{(f+1)f})}{\mu_f k_{f+1} \mathfrak{S}_{(f+1)f} \partial \bar{h}_{ff} - \mu_{f+1} k_f \partial \mathfrak{S}_{(f+1)f} \bar{h}_{ff}}, \quad (23h)$$

and the subscripts F and P denote the centrifugal and centripetal waves, respectively.

The symbols $\mathcal{T}_{(P,F)f}^H$ and $\mathcal{R}_{(P,F)f}^H$ represent the centripetal and centrifugal transmission and reflection contributions from TE waves (corresponding to the superscript H) while $\mathcal{T}_{(P,F)f}^V$ and $\mathcal{R}_{(P,F)f}^V$ represent the centripetal and centrifugal transmission and reflection contributions from TM waves (corresponding to the superscript V). The coefficients in matrix are subject to the conditions as described in Eq. (12), i.e., q and p refer to TE-mode and TM-mode, respectively.

In the same process, applying the boundary condition(4a) on the interface $r = r_0$, we can derive an equation in terms of the coefficients $\mathcal{A}_{M,N}^{fs}$ and $\mathcal{B}_{M,N}^{fs}$ as follows:

$$\begin{aligned} & \sum_{m,n} \left[(h_n^{(1)}(k_3 r_0) \mathcal{A}_{Mmn}^{35} + j_n(k_3 r_0) \mathcal{B}_{Mmn}^{35}) \mathbf{K}_{mn}^M \right. \\ & \quad \left. + \left(\frac{d[r_0 h_n^{(1)}(k_3 r_0)]}{k_3 r_0 dr_0} \mathcal{A}_{Nmn}^{35} + \frac{d[r_0 j_n(k_3 r_0)]}{k_3 r_0 dr_0} \mathcal{B}_{Nmn}^{35} \right) \mathbf{K}_{mn}^N \right] \\ & = \sum_{m,n} \left[j_n(k_4 r_0) \mathcal{B}_{Mmn}^{45} \mathbf{K}_{mn}^M + \frac{d[r_0 j_n(k_4 r_0)]}{k_4 r_0 dr_0} \mathcal{B}_{Nmn}^{45} \mathbf{K}_{mn}^N \right], \end{aligned} \quad (24)$$

where m and n on the left-hand side are so chosen that the condition as described in Eq. (12) is satisfied, and the two vectors are defined as follows:

$$\mathbf{K}_{mn}^M = (2 - \delta_m^0) \frac{2n+1}{n(n+1)} \frac{(n-m)!}{(n+m)!} \left[\frac{m}{\cos \theta} P_n^m(\cos \theta) \hat{\theta} \right]$$

$$\times \sin(m\phi) - \frac{dP_n^m(\cos\theta)}{d\theta} \sin(m\phi) \hat{\phi} \Big], \tag{25a}$$

$$\begin{aligned} \mathbf{K}_{mn}^N = & (2 - \delta_m^0) \frac{2n+1}{n(n+1)} \frac{(n-m)!}{(n+m)!} \left[\frac{dP_n^m(\cos\theta)}{d\theta} \cos(m\phi) \hat{\theta} \right. \\ & \left. - \frac{m}{\sin\theta} P_n^m(\cos\theta) \sin(m\phi) \hat{\phi} \right]. \end{aligned} \tag{25b}$$

From now on, we will add one more subscript mn to the scattering coefficients, $\mathcal{A}_{M,N}^{fs}$ and $\mathcal{B}_{M,N}^{fs}$, so as to represent different eigenvalues to be used.

Making use of the orthogonal relationships described in Appendix A for the left-hand side in Eq. (24), we can derive the following coupled equations as

$$\begin{aligned} & h_q^{(1)}(k_3 r_0) \mathcal{A}_{Mmq}^{35} + j_q(k_3 r_0) \mathcal{B}_{Mmq}^{35} \\ & = j_q(k_2 r_0) \mathcal{B}_{Mmq}^{45} + \sum_p j_p(k_4 r_0) T_{pq}^{MM} \mathcal{B}_{Mmp}^{45} \\ & + \sum_q \frac{d[r_0 j_q(k_4 r_0)]}{k_4 r_0 dr_0} T_{qq}^{MN} \mathcal{B}_{Nmq}^{45}, \end{aligned} \tag{26a}$$

$$\begin{aligned} & \frac{d[r_0 h_p^{(1)}(k_3 r_0)]}{k_3 r_0 dr_0} \mathcal{A}_{Nmp}^{35} + \frac{d[r_0 j_p(k_3 r_0)]}{k_3 r_0 dr_0} \mathcal{B}_{Nmp}^{35} \\ & = \frac{d[r_0 j_p(k_4 r_0)]}{k_4 r_0 dr_0} \mathcal{B}_{Nmp}^{45} \\ & + \sum_q \frac{d[r_0 j_q(k_4 r_0)]}{k_4 r_0 dr_0} T_{pq}^{NN} \mathcal{B}_{Nmq}^{45}, \end{aligned} \tag{26b}$$

where as $(\mathcal{P}, \mathcal{Q})$ stands for (M, N) , (M, M) , or (N, N) , we have

$$T_{ij}^{\mathcal{P}\mathcal{Q}} = \int_0^{\frac{\pi}{2}} \int_0^{2\pi} \frac{1}{\pi i(i+1) \mathcal{N}_{mi}} \mathbf{K}_{mi}^{\mathcal{P}} \cdot \mathbf{K}_{mj}^{\mathcal{Q}} \sin\theta d\theta d\phi, \tag{27}$$

with the normalized factor over $(0, \pi/2)$ given by

$$\mathcal{N}_{mn} = \int_0^{\frac{\pi}{2}} P_n^m P_n^m \sin\theta d\theta. \tag{28}$$

In a similar fashion, by applying the boundary condition (4b) on the hemi-spherical interface $r = r_0$, one more set of coupled equations can be derived as follows

$$\begin{aligned} & \frac{k_3}{\mu_3} \left[\frac{d[r_0 h_q^{(1)}(k_3 r_0)]}{k_3 r_0 dr_0} \mathcal{A}_{Mmq}^{35} + \frac{d[r_0 j_q(k_3 r_0)]}{k_3 r_0 dr_0} \mathcal{B}_{Mmq}^{35} \right] \\ &= \frac{k_4}{\mu_4} \left[\frac{d[r_0 j_q(k_4 r_0)]}{k_4 r_0 dr_0} \mathcal{B}_{Mmq}^{45} + \sum_p T_{pq}^{\prime MM} \frac{d[r_0 j_p(k_4 r_0)]}{k_4 r_0 dr_0} \mathcal{B}_{Mmp}^{45} \right. \\ & \quad \left. + \sum_q T_{qq}^{\prime MN} j_q(k_4 r_0) \mathcal{B}_{Nmq}^{45} \right], \end{aligned} \quad (29a)$$

$$\begin{aligned} & \frac{k_3}{\mu_3} \left[h_p^{(1)}(k_3 r_0) \mathcal{A}_{Nmp}^{35} + j_p(k_3 r_0) \mathcal{A}_{Nmp}^{35} \right] \\ &= \frac{k_4}{\mu_4} \left[j_p(k_4 r_0) \mathcal{B}_{Nmp}^{45} + \sum_q T_{pq}^{\prime NN} j_q(k_4 r_0) \mathcal{B}_{Nmq}^{45} \right], \end{aligned} \quad (29b)$$

where

$$T_{ij}^{\prime PQ} = \int_0^{\frac{\pi}{2}} \int_0^{2\pi} \frac{1}{\pi i(i+1) \mathcal{N}_{mi}} \mathbf{K}_{mi}^{\prime P} \cdot \mathbf{K}_{mj}^{\prime Q} \sin \theta d\theta d\phi, \quad (30)$$

in which

$$\begin{aligned} \mathbf{K}_{mn}^{\prime M} &= (2 - \delta_m^0) \frac{2n+1}{n(n+1)} \frac{(n-m)!}{(n+m)!} \left[\frac{dP_n^m(\cos \theta)}{d\theta} \sin(m\phi) \hat{\boldsymbol{\theta}} \right. \\ & \quad \left. + \frac{m}{\theta} P_n^m(\cos \theta) \cos(m\phi) \hat{\boldsymbol{\phi}} \right], \end{aligned} \quad (31a)$$

$$\begin{aligned} \mathbf{K}_{mn}^{\prime N} &= (2 - \delta_m^0) \frac{2n+1}{n(n+1)} \frac{(n-m)!}{(n+m)!} \left[-\frac{m}{\sin \theta} P_n^m(\cos \theta) \sin(m\phi) \hat{\boldsymbol{\theta}} \right. \\ & \quad \left. - \frac{dP_n^m(\cos \theta)}{d\theta} \cos(m\phi) \hat{\boldsymbol{\phi}} \right]. \end{aligned} \quad (31b)$$

B Boundary Conditions on the Aperture $z = 0$ or $\theta = \pi/2$

Now applying the boundary conditions (6) on the aperture, we can derive equations satisfied by the coefficients \mathcal{B}_{Mmn}^{45} , \mathcal{B}_{Nmn}^{45} , $C_{m\nu}^M$, and $C_{m\lambda}^N$ as follows

$$\sum_{m,n} [\mathcal{B}_{Mmn}^{45} \mathcal{F}_{mn}^M + \mathcal{B}_{Nmn}^{45} \mathcal{F}_{mn}^N] = \sum_{m,n} [C_{m\nu}^M \mathbf{u}_{m\nu}^M + C_{m\lambda}^N \mathbf{u}_{m\lambda}^N], \quad (32)$$

where

$$\begin{aligned} \mathcal{F}_{mn}^M &= \frac{ik_\nu}{4\pi} (2 - \delta_m^0) \frac{2n+1}{n(n+1)} \frac{(n-m)!}{(n+m)!} \\ &\times [-j_n(k_4r)] \left. \frac{\partial P_n^m(\cos\theta)}{\partial\theta} \right|_{\theta=\frac{\pi}{2}} \sin(m\phi) \hat{\phi}, \end{aligned} \quad (33a)$$

$$\begin{aligned} \mathcal{F}_{mn}^N &= \frac{ik_\lambda}{4\pi} (2 - \delta_m^0) \frac{2n+1}{n(n+1)} \frac{(n-m)!}{(n+m)!} \left. \frac{\partial P_n^m(\cos\theta)}{\partial\theta} \right|_{\theta=\frac{\pi}{2}} \\ &\times \left[\frac{n(n+1)}{k_4r} j_n(k_4r) \cos(m\phi) \hat{r} \right. \\ &\left. - m \frac{\partial[rJ_n(k_4r)]}{k_4r\partial r} \sin(m\phi) \hat{\phi} \right], \end{aligned} \quad (33b)$$

$$\mathcal{U}_{m\nu}^M = \frac{mJ_m(\nu\rho)}{\rho} \cos(m\phi) \hat{\rho} - \frac{dJ_m(\nu\rho)}{d\rho} \sin(m\phi) \hat{\phi}, \quad (33c)$$

$$\mathcal{U}_{m\lambda}^N = \frac{1}{k_\lambda} \left[ih \frac{dJ_m(\lambda\rho)}{d\rho} \cos(m\phi) \hat{\rho} - \frac{ihm}{\rho} J_m(\lambda\rho) \sin(m\phi) \hat{\phi} \right]. \quad (33d)$$

Again, ν and λ on the right-hand side of Eq. (32) satisfy the conditions as described in Eq. (10) while the coefficients on the left are still the same as those in Eq. (24).

By use of the orthogonal relationship described in Appendix B, the matrix equations can be derived as follows:

$$\begin{aligned} C_{m\nu}^M + 1 &= \sum_n \frac{4k_\nu}{i(2 - \delta_{m0})} \int_0^{2\pi} \int_0^{r_0} [\mathcal{B}_{Mmn}^{45} \mathcal{F}_{mn}^M \\ &+ \mathcal{B}_{Nmn}^{45} \mathcal{F}_{mn}^N] \cdot \mathcal{U}_{m\nu}^M \rho d\rho d\phi, \end{aligned} \quad (34a)$$

$$\begin{aligned} C_{m\lambda}^N + 1 &= \sum_n \frac{4k_\lambda}{i(2 - \delta_{m0})} \int_0^{2\pi} \int_0^{r_0} [\mathcal{B}_{Mmn}^{45} \mathcal{F}_{mn}^M \\ &+ \mathcal{B}_{Nmn}^{45} \mathcal{F}_{mn}^N] \cdot \mathcal{U}_{m\lambda}^N \rho d\rho d\phi, \end{aligned} \quad (34b)$$

where I_ν and I_λ have been given in Eqs. (16a–16b). It should be noted that the argument r in \mathcal{F}_{mn}^M and \mathcal{F}_{mn}^N is now reduced to ρ for the aperture opening.

In a similar fashion, using the other boundary condition on the aperture in explicit form, we have

$$\frac{k_\nu}{\mu_5} (C_{m\nu}^M + 1) = \frac{k_4}{\mu_4} \sum_n \frac{4k_\nu}{I(2 - \delta_{m0})} \int_0^{2\pi} \int_0^{r_0} [\mathcal{B}_{Mmn}^{45} \mathcal{F}_{mn}^M$$

$$\begin{aligned}
 & + \mathcal{B}_{Nmn}^{45} \mathcal{F}_{mn}'^N] \cdot \mathbf{U}'_{m\nu} \rho d \rho d \phi, \quad (35a) \\
 \frac{k_\lambda}{\mu_5} (C_{m\lambda}^N + 1) &= \frac{k_4}{\mu_4} \sum_n \frac{4k_\lambda}{I(2 - \delta_{m0})} \int_0^{2\pi} \int_0^{r_0} [\mathcal{B}_{Mmn}^{45} \mathcal{F}_{mn}'^M \\
 & + \mathcal{B}_{Nmn}^{45} \mathcal{F}_{mn}'^N] \cdot \mathbf{U}'_{m\lambda} \rho d \rho d \phi, \quad (35b)
 \end{aligned}$$

where it is defined that

$$\begin{aligned}
 \mathcal{F}_{mn}'^M &= \frac{ik_\nu}{4\pi} (2 - \delta_m^0) \frac{2n+1}{n(n+1)} \frac{(n-m)!}{(n+m)!} P_n^m(\cos\theta) \Big|_{\theta=\frac{\pi}{2}} \\
 &\times \left[\frac{n(n+1)}{k_2 r} j_n(k_2 r) \cos(m\phi) \hat{\mathbf{r}} \right. \\
 &\left. - m \frac{\partial [r j_n(k_2 r)]}{k_2 r \partial r} \sin(m\phi) \hat{\boldsymbol{\phi}} \right], \quad (36a)
 \end{aligned}$$

$$\begin{aligned}
 \mathcal{F}_{mn}'^N &= \frac{ik_3}{4\pi} (2 - \delta_m^0) \frac{2n+1}{n(n+1)} \frac{(n-m)!}{(n+m)!} \\
 &\times [-\mathfrak{S}_n(k_2 r)] \frac{\partial P_n^m(\cos\theta)}{\partial \theta} \Big|_{\theta=\frac{\pi}{2}} \sin(m\phi) \hat{\boldsymbol{\phi}}, \quad (36b)
 \end{aligned}$$

$$\mathbf{U}'_{m\nu} = \frac{1}{k_\nu} \left[ih \frac{\partial J_m(\nu\rho)}{\partial \rho} \sin(m\phi) \hat{\boldsymbol{\rho}} - \frac{hm}{\rho} J_m(\nu\rho) \cos(m\phi) \hat{\boldsymbol{\phi}} \right], \quad (36c)$$

$$\mathbf{U}'_{m\lambda} = -\frac{m J_m(\lambda\rho)}{\rho} \sin(m\phi) \hat{\boldsymbol{\rho}} - \frac{\partial J_m(\lambda\rho)}{\partial \rho} \cos(m\phi) \hat{\boldsymbol{\phi}}. \quad (36d)$$

So far, we have obtained Eqs. (19, 20, 26, 29, 34, 35) which are actually expressed in a compact matrix form. From the matrix equation system, the corresponding coefficients can be solved for and used in the future numerical computation.

5. FRAUNHOFER FIELD EXPRESSIONS IN FAR-ZONE

Consider an electric dipole polarized in the $\hat{\mathbf{r}}$ -direction located at $(\rho'', 0, -d)$ in the waveguide. The dipole current distribution is assumed to be expressed by

$$\mathbf{J}_s(\mathbf{r}') = p_r \hat{\boldsymbol{\rho}} \frac{\delta(\rho' - \rho'') \delta(\phi') \delta(z' + d)}{\rho'} \quad (37)$$

where p_r stands for the dipole moment, d denotes the distance down from dipole to aperture. For ease of computation, $\phi' = 0$ has been assumed due to the symmetry of the problem.

For the field in the far-zone region or under the high-frequency approximation $kr \gg 1$, the Hankel function and its derivative can be expressed [15] or [12] by

$$h_n^{(1)}(kr) \simeq (-i)^{n+1} \frac{e^{ikr}}{kr}, \quad (38a)$$

$$\frac{d[rh_n^{(1)}(kr)]}{dr} \simeq (-i)^n e^{ikr}. \quad (38b)$$

By making use of the above equation (38), the electric field components in the far-zone can be approximated from Eq. (2) as follows:

$$E_r \simeq \frac{E_0 r_0 e^{ikr}}{r^2} \frac{ik_s}{4\pi} \sum_{n=0}^{\infty} \sum_{m=0}^n (2 - \delta_m^0) \frac{2n+1}{n(n+1)} \frac{(n-m)!}{(n+m)!} \\ \times \mathcal{A}_M^{15} \Phi_{mn} P_n^m(\cos \theta) \sin(m\phi) \approx 0, \quad (39a)$$

$$E_\theta \simeq \frac{E_0 r_0 e^{ikr}}{r} \sum_{n=0}^{\infty} \sum_{m=0}^n (2 - \delta_m^0) \frac{2n+1}{n(n+1)} \frac{(n-m)!}{(n+m)!} \sin(m\phi) \\ \times \left[-ik \mathcal{A}_M^{15} \Phi_{mn} \frac{dP_n^m(\cos \theta)}{d\theta} + \mathcal{A}_N^{15} \Psi_{mn} \frac{P_n^m(\cos \theta)}{\sin \theta} \right], \quad (39b)$$

$$E_\phi \simeq \frac{E_0 r_0 e^{ikr}}{r} \sum_{n=0}^{\infty} \sum_{m=0}^n (2 - \delta_m^0) \frac{2n+1}{n(n+1)} \frac{(n-m)!}{(n+m)!} \cos(m\phi) \\ \times \left[-ik \mathcal{A}_M^{15} \Phi_n \frac{P_n^m(\cos \theta)}{\sin \theta} + \mathcal{A}_N^{15} \Psi_n \frac{dP_n^m(\cos \theta)}{d\theta} \right], \quad (39c)$$

where

$$\Phi_{mn} = \iiint_V \mathbf{M}'_{\epsilon_{m\nu}}(-k_\nu) \cdot \mathbf{J}_s(\mathbf{r}') dV' \\ = \left. \frac{p_r m J_m(\nu \rho')}{\rho'} \right|_{\rho'=\rho''} e^{i h d}, \quad (40a)$$

$$\Psi_{mn} = \iiint_V \mathbf{N}'_{\epsilon_{m\lambda}}(-k_\lambda) \cdot \mathbf{J}_s(\mathbf{r}') dV' \\ = - \left. \frac{p_r h \partial J_m(\lambda \rho')}{k_\lambda \partial \rho'} \right|_{\rho'=\rho''} e^{i h d}. \quad (40b)$$

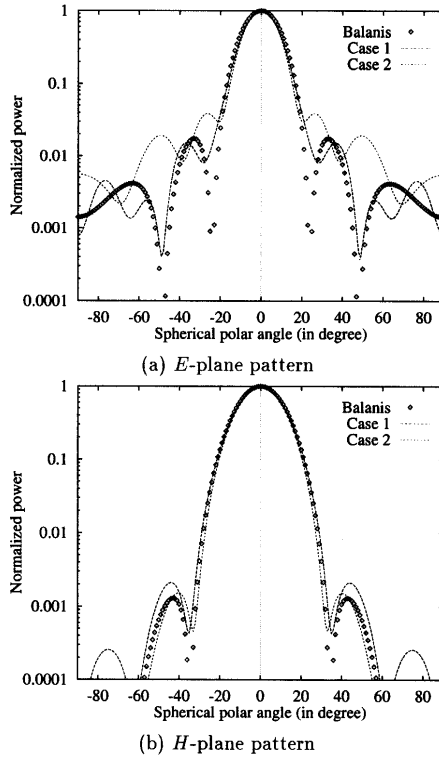


Figure 2. Normalized power patterns against spherical polar angle for three different situations: (i) Balanis where there is no radome and reaction feed-back effects are absent; (ii) Case 1 where the radome is absent but the full-wave analysis is considered; and (iii) Case 2 where the radome is present and the full-wave analysis is considered.

6. NUMERICAL DISCUSSIONS ON EFFECTS OF APERTURE-RADOME INTERACTION

The power patterns at a frequency of 3 GHz are obtained numerically, as shown in Fig. 2. Three cases are considered in Fig. 2, namely (i) “*Balanis*” — the Balanis’s radome-free result for which the given source distribution *without field feed-back* is assumed; (ii) “*Case 1*” — a radome-free result for which the full-wave analysis is considered; and (iii) “*Case 2*” — a result for which the radome is present and the

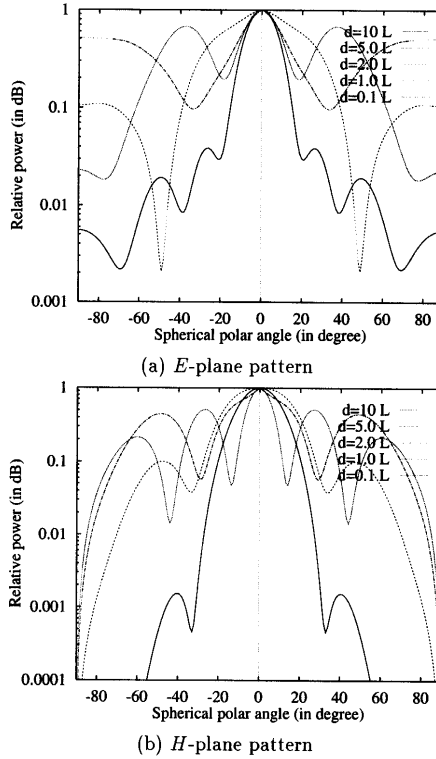


Figure 3. Normalized power patterns of far zone fields against spherical polar angle θ for various positions where the dipole locates in the waveguide. $L = \lambda_e$ is the wavelength of waves in the dielectric radome.

full-wave analysis is considered. The parameters used in the particular discussion are: the aperture radius, $r_0 = 1.5\lambda_0$; the inner radius of the radome, $a = 1.5\lambda_0$; the thickness of the radome, $d = \lambda_e/2$; and the relative permittivity of the radome material, $\epsilon_r = 4.6(1 + i0.023)$ where the relative permittivity and the wavelength in radome material are given generally by $\epsilon_r = \epsilon'(1 + \tan \delta i)$ and $\lambda_e = \lambda_0/\sqrt{\epsilon'}$, respectively. It can be seen clearly that the main lobe and the null beam widths of the aperture antenna pattern become narrow in the presence of the radome. Of special interest is the observation that the radome

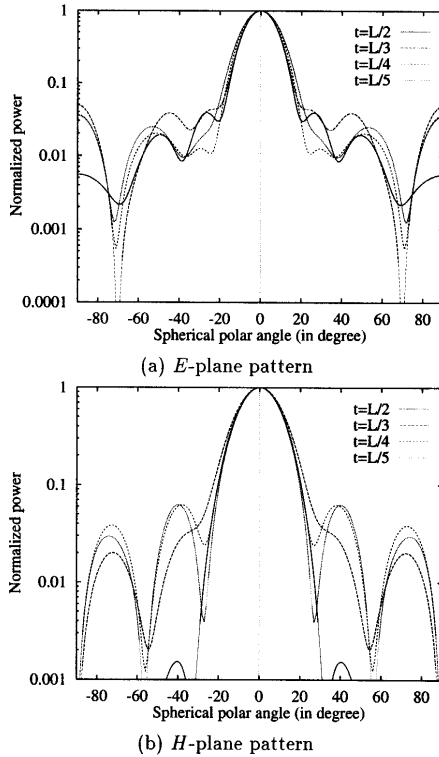


Figure 4. Normalized power patterns of far zone fields against spherical polar angle θ for various radome thicknesses. $L = \lambda_e$ is the wavelength in the dielectric radome.

causes the side lobes of higher power level especially near an angle of θ from 80° to 90° . This is mainly due to the effects of high modes.

To gain insight into the effects of the dipole location on the power pattern, Fig. 3 shows the normalized E - and H -plane patterns against the spherical polar angle. It is assumed that d , which is the distance from dipole to waveguide opening, changes from $0.1\lambda_e$ to $10\lambda_e$. The parameters used are still the same as those in Fig. 2. When the distance is extremely large, the power patterns represent the far-zone pattern, therefore remain the same even if the distance gets larger. It can also be seen that as the dipole moves toward the opening of the waveguide, the

power patterns become more complicated. This is expected as more multiple interactions between the dipole antenna and the waveguide opening (such as the strong diffraction) come to be significant. More and high side lobes and poor direction occur on the patterns for this case, because of the high-order modes.

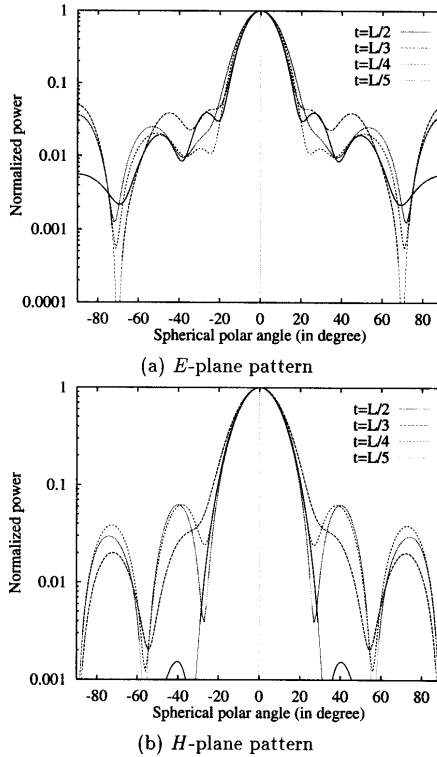


Figure 5. Power patterns of far zone fields against spherical polar angle θ for various radome inner radii, where $a_2 = 1.5\lambda_0 \left(1 + \frac{n}{4}\right)$ ($n = 0, 1, 2, 3$ and 4).

Fig. 4 shows another example where the effects of the radome thickness t have been taken into account. The parameters used are still the same as before in Fig. 2. It is realized that the *E*- and *H*-plane patterns of the excited aperture in the presence of a radome with half-wave thickness resemble those in the absence of radome. Physically,

this is what we expected from the considerations of transmission line theory. When the thickness $t \neq n\lambda_e/2$ (for instance, it becomes less than a half wavelength), the radiation pattern gets distorted as the impedance matching is broken. As a result, more multiple reflections make the high-order modes present and then form the higher flash lobes near $\theta = 80^\circ - 90^\circ$.

To gain insight into the effects of the radome inner radius, Fig. 5 shows the normalized E - and H -plane patterns against the spherical polar angle. It is assumed that $a_2 = 1.5\lambda_0(1 + \frac{n}{4})$ where n changes from 0 to 4), while the aperture size r_0 is still equal to $1.5\lambda_0$. It is apparent that for a half-wave radome thickness (i.e. $t = \lambda_e/2$), the power patterns do not change with the radome inner radius significantly, as shown in Fig. 4. However, the multiple reflections can be very strong if the radius of the radome is close to the dimension of the aperture opening, which is not desirable.

7. CONCLUDING REMARKS

This paper presents a rigorous full-wave analysis of the antenna radiation inside a conducting waveguide that is covered by a dielectric hemi-spherical radome over the ground plane. Both the electromagnetic fields radiated by the antenna located inside the waveguide and the dyadic Green's functions in such a structure are formulated. The scattering superposition principle and the mode-matching technique are applied. The scattering coefficients of the dyadic Green's functions, although coupled in matrix form, are derived by matching the boundary conditions on circular waveguide conducting walls and all the dielectric interfaces. Furthermore, the Fraunhofer electric fields are obtained using the far-zone approximation. As a demonstration on how the theory is implemented in practical applications, the E -plane and H -plane power patterns of the open aperture excited by a dipole antenna located inside the circular waveguide are obtained and computed for various dimensions of the radiating system.

The results currently obtained are compared with existing published data. In the comparison made, the result of Balanis [1] (in the case of TE_{11} wave excitation without field feed-back and in the absence of a radome) is considered as a base. The following conclusions can be drawn from the analysis and the comparisons.

- The main lobe and the null beam widths of the aperture antenna pattern become narrow in the presence of a radome. Of special interest is the observation that the radome causes the side lobes of higher power level, especially near an angle of θ from 80° to 90° .
- As the dipole becomes nearer to the aperture, the field patterns become more complicated. More side lobes and poor direction occur. It is realized that the multiple interaction between the dipole antenna and the aperture opening results in significant changes in power patterns.
- The thickness of the dielectric radome plays an important role in the radome design and a half-wave thickness is the best choice of the radome thickness since it is almost transparent to the radio wave radiated from the centre-located aperture; a radome of thickness thinner than half-a-wavelength bears even more transmission loss and makes the power patterns rather dramatic.
- For a given radome thickness of $\lambda_e/2$, the field patterns are almost independent of the radome inner radius when the radius has been quite large. However, quite small radome, which has a radius close to the aperture dimension, can also significantly distort the performance of the antenna system.

A ORTHOGONAL RELATIONS OF THE CONICAL VECTOR WAVE FUNCTIONS

Following the method described in Tai [12] and using integration by parts for half space, it is not difficult to show that

$$\int_0^{\pi/2} \left[\left(\frac{dP_q^m}{d\theta} \right)^2 + \left(\frac{mP_q^m}{\sin \theta} \right)^2 \right] \sin \theta d\theta = q(q+1)I_{mq}, \quad (\text{A1a})$$

$$\int_0^{\pi/2} \left[\left(\frac{dP_p^m}{d\theta} \right)^2 + \left(\frac{mP_p^m}{\sin \theta} \right)^2 \right] \sin \theta d\theta = p(p+1)I_{mp}, \quad (\text{A1b})$$

where

$$\int_0^{\pi/2} P_q^m P_{q'}^m \sin \theta d\theta = \begin{cases} 0, & q \neq q' \\ I_{mq}, & q = q' \end{cases}, \quad (\text{A2a})$$

$$\int_0^{\pi/2} P_p^m P_{p'}^m \sin \theta d\theta = \begin{cases} 0, & p \neq p' \\ I_{mp}, & p = p' \end{cases}, \quad (\text{A2b})$$

and

$$\begin{cases} q, & q + m = \text{even for } \mathbf{M}_{\circ mn}\text{-mode;} \\ p, & p + m = \text{odd for } \mathbf{N}_{\circ mn}\text{-mode.} \end{cases} \quad (\text{A3})$$

With the aid of these orthogonal relations, the orthogonal relations of the conical vector wave functions can be determined as follows:

$$\iiint \mathbf{M}_{\circ mq}(\kappa) \cdot \mathbf{N}_{\circ m'p'}(\kappa') dV = 0; \quad (\text{A4a})$$

$$\iiint \mathbf{M}_{\circ mp}(\kappa) \cdot \mathbf{N}_{\circ m'p'}(\kappa') dV = 0; \quad (\text{A4b})$$

$$\begin{aligned} & \iiint \left\{ \begin{array}{l} \mathbf{M}_{\circ mq}(\kappa) \cdot \mathbf{M}_{\circ m'q'}(\kappa') \\ \mathbf{N}_{\circ mq}(\kappa) \cdot \mathbf{N}_{\circ m'q'}(\kappa') \end{array} \right\} dV \\ &= \begin{cases} 0, & m \neq m' \text{ or } q \neq q', \\ \frac{(1 + \delta_0)\pi^2 q(q + 1)I_{mq}}{2k^2} \delta(\kappa - \kappa') & m = m' \ \& \ q = q'; \end{cases} \quad (\text{A4c}) \end{aligned}$$

$$\begin{aligned} & \iiint \left\{ \begin{array}{l} \mathbf{M}_{\circ mp}(\kappa) \cdot \mathbf{M}_{\circ m'p'}(\kappa') \\ \mathbf{N}_{\circ mp}(\kappa) \cdot \mathbf{N}_{\circ m'p'}(\kappa') \end{array} \right\} dV \\ &= \begin{cases} 0, & m \neq m' \text{ or } p \neq p', \\ \frac{(1 + \delta_0)\pi^2 p(p + 1)I_{mp}}{2k^2} \delta(\kappa - \kappa') & m = m' \ \& \ p = p'. \end{cases} \quad (\text{A4d}) \end{aligned}$$

B ORTHOGONAL RELATIONS OF CYLINDRICAL VECTOR WAVE FUNCTIONS

The orthogonal Relations between the various cylindrical vector wave functions can be stated as follows [12]:

$$\iiint \mathbf{M}_{\circ m\nu}(h) \cdot \mathbf{N}_{\circ m'\lambda}(-h') dV = 0; \quad (\text{B5a})$$

$$\begin{aligned} & \iiint \mathbf{M}_{\circ m\nu}(h) \cdot \mathbf{M}_{\circ m'\nu'}(-h') dV = \iiint \mathbf{N}_{\circ m\nu}(h) \cdot \mathbf{N}_{\circ m'\nu'}(-h') dV \\ &= \begin{cases} 0, & m \neq m' \text{ or } \nu \neq \nu', \\ (1 + \delta_0)2\pi^2 \nu^2 I_{m\nu} \delta(h - h'), & m = m' \ \& \ \nu = \nu'; \end{cases} \quad (\text{B5b}) \end{aligned}$$

$$\begin{aligned} & \iiint \mathbf{M}_{\circ m\lambda}(h) \cdot \mathbf{M}_{\circ m'\lambda'}(-h') dV = \iiint \mathbf{N}_{\circ m\lambda}(h) \cdot \mathbf{N}_{\circ m'\lambda'}(-h') dV \\ &= \begin{cases} 0, & m \neq m' \text{ or } \lambda \neq \lambda', \\ (1 + \delta_0)2\pi^2 \lambda^2 I_{m\lambda} \delta(h - h'), & m = m' \ \& \ \lambda = \lambda'. \end{cases} \quad (\text{B5c}) \end{aligned}$$

ACKNOWLEDGMENT

This work was supported in part by a grant under the MINDEF/NUS Joint Project 12/13/96.

REFERENCES

1. Balanis, C. A., *Antenna Theory: Analysis and Design*, John Wiley & Sons. New York, The 2nd edition, 1997.
2. Stutzman, W. L., and G. A. Thiele, *Antenna Theory and Design*, John Wiley & Sons, New York, 2nd edition, 1998.
3. Kraus, J. D., *Antennas*, McGraw-Hill, New York, The 2nd edition, 1981.
4. Li, L. W., P. S. Kooi, M. S. Leong, T. S. Yeo, and X. Ma, "An analysis of a circular aperture antenna covered with a dielectric hemi-spherical shell radome over ground plane," in *Digest of 1995 IEEE AP-S International Symposium and USNC/URSI Radio Science Meeting*, Vol. 3rd of 4, 1442–1445, Newport Beach, California, USA, June 18–23, 1995.
5. Leong, M. S., L. W. Li, X. Ma, P. S. Kooi, and T. S. Yeo, "Effects of rainfall on total transmission loss and cross-polarization of a hemi-spherical dielectric radome with rain-water layer: A closed form solution," *J. Electromagn. Waves Applic.*, Vol. 12, No. 6, 731–752, June 1998.
6. Li, L. W., P. S. Kooi, M. S. Leong, and T. S. Yeo, "Electromagnetic dyadic Green's function in spherically multilayered media," *IEEE Trans. Microwave Theory Tech.*, Vol. 42, No. 12, 2302–2310, December 1994, Part A.
7. Li, L. W., M. S. Leong, P. S. Kooi, T. S. Yeo, and Y. L. Qiu, "Radiation of an aperture antenna covered by a spherical shell chiral radome and fed by a circular waveguide," *IEEE Trans. on Antennas Propagat.*, Vol. 46, No. 5, 664–671, May 1998.
8. Leong, M. S., L. W. Li, X. Ma, P. S. Kooi, and T. S. Yeo, "Radiation characteristics of a circular aperture covered asymmetrically by a dielectric hemispherical radome," in *1996 IEEE Singapore International Conference on Communications Systems*, (ICCS'96), Vol. 1st of 3, 277–281, Singapore, November 25–29, 1996.
9. Li, L. W., M. S. Leong, L. Zhou, P. S. Kooi, and T. S. Yeo, "A novel analysis of antenna radiation from a circular aperture covered by a dielectric hemi-spherical radome shell," in *The 1998 International Wireless and Communications Symposium/Exhibition*, PWTC, Kuala Lumpur, May 11–15, 1998.

10. Collin, R. E., *Field Theory of Guided Waves*, IEEE Press, Piscataway, New Jersey, The 2nd edition, 1991.
11. Chew, W. C., *Waves and Fields in Inhomogeneous Media*, Van Nostrand Reinhold, New York, 1990.
12. Tai, C. T., *Dyadic Green's Functions in Electromagnetic Theory*, IEEE Press, Piscataway, New Jersey, The 2nd edition, 1994.
13. Ali, S. M., T. M. Habashy, and J. A. Kong, "Spectral-domain dyadic Green's function in layered chiral media," *J. Opt. Soc. Am. A.*, Vol. 9(3), 413–423, 1992.
14. Li, L. W., J. A. Bennett, and P. L. Dyson, "Some methods for solving the coefficients of dyadic Green's function in isotropic stratified media," *Int. J. Electron.*, Vol. 70(4), 803–814, 1991.
15. Stratton, J. A., *Electromagnetic Theory*, McGraw-Will, New York, 1941.